




Article

Comparison of Biochar Materials Derived from Coconut Husks and Various Types of Livestock Manure, and Their Potential for Use in Removal of H₂S from Biogas

Lianghu Su ¹, Mei Chen ¹, Guihua Zhuo ², Rongting Ji ¹, Saier Wang ^{1,*}, Longjiang Zhang ¹, Mingzhu Zhang ^{1,*} and Haidong Li ¹

¹ Nanjing Institute of Environmental Sciences, Ministry of Ecology and Environment, Nanjing 210042, China; sulianghu@nies.org (L.S.); chenmei@nies.org (M.C.); jirongting@nies.org (R.J.); zlj@nies.org (L.Z.); lihd2020@163.com (H.L.)

² Fujian Provincial Academy of Environmental Science, Fuzhou 350003, China; zhuoguihua_1985@126.com

* Correspondence: wangsaier@nies.org (S.W.); zhangmingzhu@nies.org (M.Z.); Tel.: +86-025-852-87-439 (S.W.); +86-025-852-87-298 (M.Z.)

Abstract: As a potential adsorbent material, loose, porous livestock manure biochar provides a new approach to livestock manure resource utilization. In this study, coconut husks (CH) and livestock manure, i.e., cow dung (CD), pig manure (PM), and chicken manure (CM) were used as biomass precursors for preparation of biochar via high-temperature pyrolysis and CO₂ activation. Characterization technologies, such as scanning electron microscopy, Fourier transform infrared spectroscopy, adsorption–desorption isotherms, and pore size distributions, were used to study the microscopic morphologies and physicochemical properties of unactivated and activated biochar materials. The results showed that CD biochar provides better adsorption performance (up to 29.81 mg H₂S/g) than CM or PM biochar. After activation at 650° for 1 h, the best adsorption performance was 38.23 mg H₂S/g. For comparison, the CH biochar removal performance was 30.44 mg H₂S/g. Its best performance was 38.73 mg H₂S/g after 1 h of activation at 750 °C. Its best removal performance is equivalent to that of CH biochar activated at a temperature that is 100 °C higher. Further material characterization indicates that the H₂S removal performance of livestock-manure-derived biochar is not entirely dependent on the specific surface area, but is closely related to the pore size distribution.

Keywords: livestock manure; Biochar; physical activation; hydrogen sulfide removal



Citation: Su, L.; Chen, M.; Zhuo, G.; Ji, R.; Wang, S.; Zhang, L.; Zhang, M.; Li, H. Comparison of Biochar Materials Derived from Coconut Husks and Various Types of Livestock Manure, and Their Potential for Use in Removal of H₂S from Biogas. *Sustainability* **2021**, *13*, 6262. <https://doi.org/10.3390/su13116262>

Academic Editor: Bing Wang

Received: 1 May 2021

Accepted: 31 May 2021

Published: 1 June 2021

Publisher's Note: MDPI stays neutral with regard to jurisdictional claims in published maps and institutional affiliations.



Copyright: © 2021 by the authors. Licensee MDPI, Basel, Switzerland. This article is an open access article distributed under the terms and conditions of the Creative Commons Attribution (CC BY) license (<https://creativecommons.org/licenses/by/4.0/>).

1. Introduction

More than 7 billion tons of livestock manure is produced in China each year. The amount of livestock manure produced is increasing at an annual rate of about 10% [1]. With the rapid development of modern livestock and poultry breeding techniques, livestock manure pollution has become a worldwide problem [2,3]. Livestock manure that contains large amounts of pathogenic bacteria not only causes water eutrophication and soil pollution, but also causes serious harm to human, livestock, and poultry health [4,5]. As an alternative to traditional composting and anaerobic digestion, pyrolysis treatment of livestock manure can effectively reduce the environmental burden imposed while providing a high value-added product. Thus, it represents a promising resource utilization method [6,7].

Pyrolysis of livestock manure is the process of converting livestock manure into biochar, tar, and pyrolysis gas at high temperatures (>400 °C) under oxygen-limited conditions [8,9]. With a porous structure and large specific surface area, the biochar obtained from pyrolysis is a highly aromatic solid substance with good adsorption of metal pollutants, organic pollutants, etc. [10]. Although the specific surface area of livestock-manure-derived biochar is not high compared to that of biochar derived from other biomass sources, it

tends to improve dramatically after activation [11]. In addition, the high salt content of livestock manure causes functional groups to remain on the surface after pyrolysis. This may enhance its adsorption capacity [12,13]. Therefore, livestock manure biochar is often used as a soil remediation agent [14–16]. For example, Meier et al. used alkaline chicken-manure-derived biochar to increase the soil pH in order to reduce the mobility of Cu and adsorb it, thereby effectively repairing soil that was contaminated by heavy metals [17]. Given its high porosity and specific surface area, livestock manure biochar may be a suitable gas adsorption material. However, few researchers have studied it.

Desulfurization treatment is required before comprehensive utilization of biogas, otherwise highly toxic hydrogen sulfide gas that is produced corrodes metal pipes in oxygen-rich and humid environments, shortens the service life of internal combustion engines and compressors, and causes damage to seals [18–20]. As a lower cost, higher efficiency desulfurization technology, biochar adsorption has received widespread attention [21,22]. Hervy et al. prepared an alkaline biochar from food residues via gas-phase oxidation and steam activation. The product had a removal capacity of 65 mg H₂S/g under dry syngas, and the study demonstrated that surface formation of metal sulfides and metal sulfates effectively improves the H₂S removal efficiency [23]. Microporous bamboo biochar prepared by Yang et al. via pyrolysis and ZnCl₂ activation exhibited a maximum adsorption capacity and breakthrough capacity of 38.4 mg H₂S/g and 9.5 mg H₂S/g [24]. Although it is a promising adsorption material, few studies have focused on the H₂S removal performance of livestock manure biochar. Choosing the correct activation method and temperature is critical to developing the removal performance of livestock manure biochar [25,26].

The purpose of this study was to evaluate the desulfurization performance of livestock manure biochar and to provide innovative methods of using this resource. Herein, three types of livestock manure were used as biomass precursors in biochar preparation via pyrolysis. Coconut husk was also pyrolyzed for comparison. The H₂S adsorption performances of the various biochar samples were then evaluated. CO₂ physical activation was applied, and the ability of livestock manure biochar to remove H₂S after activation at temperatures from 650 to 850 °C was evaluated further. In addition, X-ray diffraction, thermogravimetry, infrared spectroscopy, scanning electron microscopy, specific surface area, and pore size analyses were used to detail the relationships between biochar sample physicochemical characteristics and their H₂S removal abilities.

2. Materials and Methods

2.1. Test Materials

Various types of livestock manure, i.e., cow dung (CD), pig manure, (PM), and chicken manure (CM) were obtained from various livestock and poultry farms in Jiangsu Province. Coconut husk (CH) was from a coconut product processing plant in Hainan Province, China. Quartz wool (5–9 µm) was purchased from Aladdin Co. Ltd. in China. Quartz sand (100 mesh) was purchased from Qingdao Uoslf Chemical Technology Co., Ltd.

2.2. Biochar Preparation and Activation Procedure

The biochar preparation and activation unit setup is shown in Figure 1. For biochar preparation, various types of livestock manure and coconut husk were dried thermally at 65 °C for 24 h, and biochar was produced via slow pyrolysis. Specifically, thermally dried livestock manure and coconut husk were loaded into the reactor and heated at the rate of 20 °C min⁻¹ under N₂ atmosphere. A tubular furnace (RD 30, Nabertherm GmbH, Germany) was used to control the temperature. After pyrolysis at 500 °C for 60 min under N₂, the samples were allowed to cool naturally to room temperature over the course of 24 h. The prepared CH, CD, PM, and CM biochar samples were recorded as CH-500P, CD-500P, PM-500P, and CM-500P, respectively. For activation, these biochar samples were loaded into the reactor and heated at the rate of 20 °C min⁻¹ under N₂. Once the activation temperature was reached, CO₂ was introduced into the system. The biochar was activated at various temperatures for various times at a flow rate of 200 mL/min.

The CH-500C, CD-500C, PM-500C, and CM-500C biochar samples activated at 650 °C, 750 °C, and 850 °C were recorded as CH-500P-650A, CD-500P-650A, PM-500P-650A, and CM-500P-650; CH-500P-750A, CD-500P-750A, PM-500P-750A, and CM-500P-750A; and CH-500P-850A, CD-500P-850A, PM-500P-850A, and CM-500P-850 A.

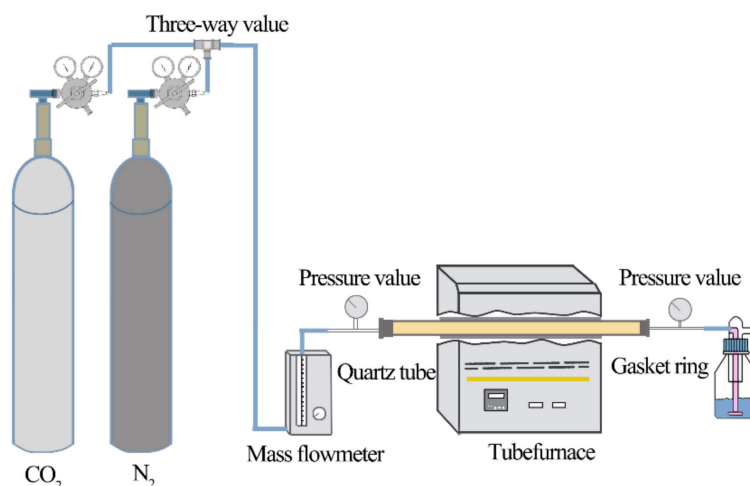


Figure 1. Biochar preparation and activation unit setup.

2.3. H₂S Removal Experiment

H₂S removal tests were performed in a custom-designed quartz fixed-bed reactor, as reported in our previous studies [27,28] and shown in Figure 2. A mass flowmeter (S48 32/HMT, Horiba Metron, China) was used to control the biogas flow into the quartz column. The reactor exit was connected to a six-port Valco GC valve (VICI, Valco, Houston, TX, USA) and the H₂S concentration was monitored on-line (every 6.2 min) using a gas chromatograph (Sp-3420A, Beijing BFR Analytical Instrument Co., Ltd., China) equipped with a flame ionization detector (FID) and a Hayesep R column (4'×1/8'). The breakthrough capacity was determined at an exit H₂S concentration equal to 30% of the inlet concentration. All reactions were performed under a fume hood due to the high toxicity of H₂S. Exactly 0.20 g of biochar and 0.80 g of 100-mesh quartz sand were mixed adequately to avoid the possibility of channelling, and then packed in a quartz column (8 mm, i.d., and a fixed height of 270 mm). Quartz wool was packed at the bottom and top of the biochar/quartz sand mixture to facilitate gas diffusion. A synthetic mix of CH₄ (60%), CO₂ (39%), and H₂S (1%) was provided by Nanjing Tianze Gas Co. Ltd. The H₂S removal capacities, expressed as x/M (mg H₂S g⁻¹ of material), were calculated by integrating the corresponding breakthrough curves and applying Equation (1):

$$\frac{x}{M} = \frac{Q \times MW}{w \times V_M} (c_0 \times t_s - \int_0^{t_s} c(t) dt) \quad (1)$$

where Q is the inlet flow rate (m³ s⁻¹), w is the weight of biochar introduced into the column (g), MW is the molecular weight of H₂S (34 g mol⁻¹), V_M is the molar volume (22.4 L mol⁻¹), c₀ is the inlet gas H₂S concentration (ppm_v), c(t) is the gas outlet concentration (ppm_v), and t_s is the bed saturation or exhaustion time (s). To achieve statistical quality, H₂S removal experiments were performed in duplicate using each of the samples, and average x/M values were calculated.

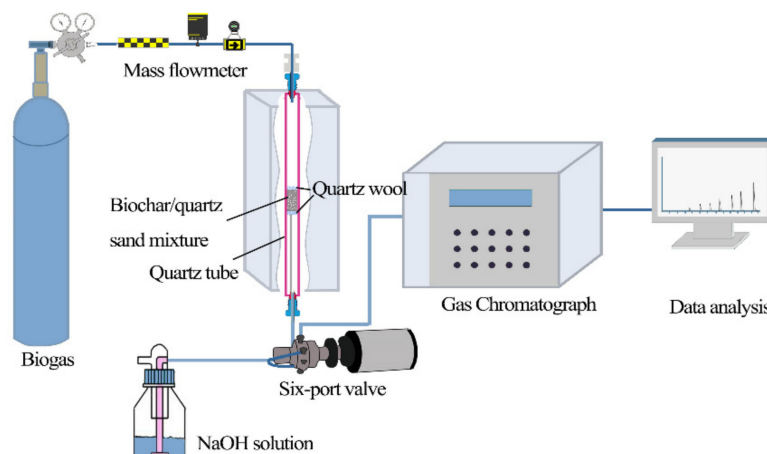


Figure 2. Schematic description of the experimental laboratory apparatus.

2.4. Analytical Methods

An AD-8-Advance X-ray diffractometer (Bruker AXS Inc., Germany), with an accelerating voltage of 40 kV and a current of 40 mA, was used for powder X-ray diffraction (PXRD) analysis. The samples were examined at room temperature over a 2θ range of $10\text{--}90^\circ$ using graphite-monochromated $\text{Cu K}\alpha$ radiation. The scan step was 0.02° and the measurement time increments were 0.01 s step^{-1} . Diffractograms were obtained using Diff-plus and analysed using MDI Jade 5.0 software.

The microscopic morphologies of the samples were analyzed via scanning electron microscopy (SEM, SUPRA55, Germany). The working voltage was 1–30 kV, the point resolution was 3.5 nm, the magnification was $10\times\text{--}300,000\times$, the sample stage tilt angle was $10\text{--}80^\circ$, secondary electron and backscatter detectors were used, and the heating stage temperature range was varied between room temperature and 600°C . Thermogravimetric analysis and differential thermogravimetric analysis (TGA/DTG) were performed using an SDT Q600 simultaneous thermal analyzer (TA, USA). The samples were heated from 50 to 700°C at $10^\circ\text{C min}^{-1}$ under a nitrogen flow (100 mL min^{-1}). Elemental compositions (C, H, S, and N) were analyzed using a FLASH2000 organic element analyzer. Heavy metal content analysis was performed via ICP–OES (Varian 7100, Agilent Technologies, Inc) after acid digestion pretreatment of the sample. For pH analysis, 10 g of biochar and activated product were added to 100 mL of deionized water, and the pH values were measured by a pH meter (model PHS-3C, China). N_2 isotherms were measured using a Micromeritics TriStar 3000 analyzer at -198°C . Before analysis, the samples were degassed at 350°C for 4 h. The Brunauer–Emmett–Teller (BET) and Langmuir surface areas were calculated using the BET and Langmuir equations, respectively.

3. Results and Discussions

3.1. Characteristics of Coconut Husks and Various Types of Livestock Manure

The biomass precursors used in this study included CD, PM, and CM, with CH used for comparative purposes. The physical and chemical properties of various biomass precursors are shown in Table 1. The pH of CH is neutral, while PM, CM, and CD are alkaline (10.05–10.55). With high salt contents, the three kinds of livestock manure have higher conductivities than CH ($2.09 \mu\text{s/cm}$). Of the three types of manure, CD has the highest conductivity ($8.73 \mu\text{s/cm}$). CM has the highest density (0.776 g/cm^3) and CD has the lowest density (0.418 g/cm^3). In addition, CH and CD contain more organic matter with higher volatile solid (VS) content (78.8–96.2%). Elemental analysis shows that PM has the highest heavy metal content, including a Zn content of 2.23 mg/g and Cu content of 0.58 mg/g . This may be attributed to feed additives [28]. CD and CM have the highest K contents (41.75 mg/g and 13.16 mg/g , respectively). PM and CM have the highest Ca contents at 26.46 mg/g and 65.44 mg/g , respectively. The P contents of the various raw

materials are quite different. The P contents of CM and PM are high at 12.88 mg/g and 10.73 mg/g, respectively, while the P contents of CH and CD are lower at 0.64 mg/g.

Table 1. Characteristics of coconut husks and various types of livestock manure.

Parameter	CH	CD	PM	CM
pH	6.15 ± 0.07	10.55 ± 0.01	10.05 ± 0.02	10.34 ± 0.04
EC (µs/cm)	2.09 ± 0.04	8.73 ± 0.48	4.23 ± 0.13	3.45 ± 0.16
Moisture content (%)	15.09 ± 0.30	11.64 ± 0.41	12.93 ± 0.13	8.30 ± 0.11
VS (%)	96.16 ± 0.02	78.83 ± 2.00	69.82 ± 0.61	40.66 ± 1.01
Density (g/cm ³)	0.428	0.418	0.757	0.776
Si (mg/g)	0.15	0.95	0.96	1.65
Fe (mg/g)	0.46	2.05	3.51	9.56
Ca (mg/g)	1.36	17.93	26.46	65.44
Al (mg/g)	0.09	0.54	1.20	2.97
Na (mg/g)	1.18	8.67	2.63	1.83
Mg (mg/g)	0.63	6.35	6.98	7.57
K (mg/g)	6.90	41.75	12.05	13.16
Zn (mg/g)	0.03	0.18	2.23	0.21
Cu (mg/g)	0.03	0.04	0.58	0.04
Cr (mg/g)	0.01	0.07	0.16	0.36
Mn (mg/g)	0.01	0.17	0.50	0.42
Ba (mg/g)	0.04	0.03	0.03	0.06
Ni (mg/g)	0.06	<0.01	0.01	0.02
Cd (mg/g)	<0.01	<0.01	<0.01	<0.01
P (mg/g)	0.64	0.64	12.88	10.73

In order to further understand the inorganic components of each raw material, PXRD was used to characterize each biomass precursor. As shown in Figure 3a, livestock manure contains inorganic salts, the main components of which are SiO₂ and CaCO₃, but few inorganic salt diffraction peaks are observed from the coconut husks [29]. TGA was performed to characterize the thermal stability of the biomass precursor. As shown in Figure 3b, the biomass precursor weight loss process is divided into two main stages. The first stage ranges from 50 to 250 °C and features loss of residual water molecules (5.33%, 8.50%, 7.90%, and 3.24% of the total masses of CH, CD, PM, and CM, respectively). Most thermal weight loss from the biomass precursor occurs at 300 to 400 °C. Weight loss from CH, CD, PM, and CM within this temperature range is 61.59%, 47.66%, 43.38%, and 17.38%, respectively. For chicken manure, significant weight loss occurs in the 600 °C to 700 °C range. This may be attributed to decomposition of CaCO₃. The second stage of thermal weight loss corresponds to the decomposition of organic matter. Thus, one can conclude that CH has the highest organic matter content. This is consistent with the vs. characterization results. The organic matter content of the livestock manure follows the order CD > PM > CM.

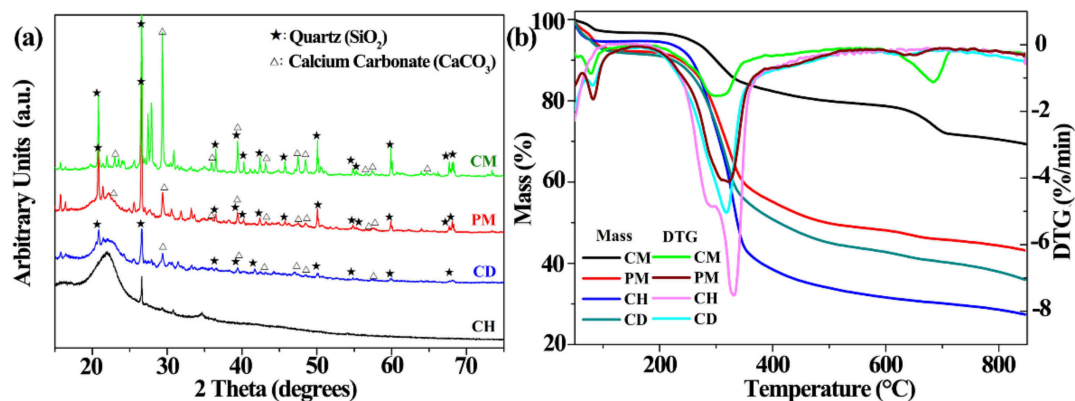


Figure 3. (a) PXRD spectra of the crystalline phases of coconut husks and various types of livestock manure; (b) TG and DTG curves from coconut husks and various types of livestock manure.

3.2. Characteristics of Livestock Manure Biochar and Activated Biochar

The surface pH, density, BET surface area, ignition loss rate, and other prepared biochar sample parameters are characterized and shown in Table 2. The surface pHs of CH-500C and CD-500C are the highest at 10.5, while that of PM-500C is the lowest at 9.5. When the biochar surface pH exceeds 5.0, it may have a substantial H₂S adsorption capacity [30]. The N₂ adsorption–desorption analysis results show that the surface areas and pore volumes of biochars prepared with various biomass precursor properties are significantly different. The specific surface areas of the biochars follow the order: CM-500C (11.84 m²/g) > CD-500C (7.01 m²/g) > PM-500C (6.89 m²/g) > CH-500C (0.18 m²/g). CM-500C has the largest bulk density (0.769 g/cm³) and the lowest ignition loss rate (29.28%); CH-500C and CM-500C have the smallest bulk densities (0.415 g/cm³), and coconut husk biochar has the largest ignition loss rate (79.37%). The burning loss rate of cow dung biochar is also high at 64.95%. The volumetric densities of the prepared biochar materials decrease as the ash content increases. The ash content is inversely proportional to the ignition loss rate and is related to the pyrolysis temperature [31].

Table 2. Physical and chemical characteristics of prepared biochars.

Sample	pH	BET (m ² /g)	Density (g/cm ³)	Burn Off (%)
CH-500P	10.5	0.18	0.415	79.37
CD-500P	10.5	7.01	0.415	64.95
PM-500P	9.5	6.89	0.752	57.07
CM-500P	9.7	11.84	0.769	29.28

The surface pH, density, BET surface area, ignition loss rate, and other activated biochar parameters were characterized and are shown in Table 3. The biochar density and pH change little with the activation temperature. The specific surface area of CH-500P increases with the temperature. The specific surface area is largest (811.46 m²/g) when the activation temperature is 850 °C. The ignition loss rate is 75.04%. However, increasing the activation temperature causes the specific surface areas of CM-500P and CD-500P to decrease, while that of PM-500P first increases and then decreases. The livestock manure samples with the largest specific surface areas after activation are: CD-500P-650A (130.80 m²/g), PM-500P-750A (125.80 m²/g), and CM-500P-650A (23.55 m²/g).

Table 3. Physical and chemical properties of biochar samples after activation at various temperatures.

Sample	pH	Surface Area		Density (g/cm ³)	Burn Off (%)
		BET (m ² /g)	Langmuir (m ² /g)		
CH-500P-650A	10.4	331.86	491.07	0.413	21.29
CD-500P-650A	10.4	130.80	197.03	0.399	29.45
PM-500P-650A	9.6	70.54	104.79	0.707	14.60
CM-500P-650A	9.4	23.55	35.56	0.758	11.37
CH-500P-750A	10.3	604.13	898.55	0.398	36.05
CD-500P-750A	10.3	11.28	17.74	0.395	55.95
PM-500P-750A	9.4	125.80	188.86	0.709	22.15
CM-500P-750A	10.3	10.45	15.78	0.755	21.13
CH-500P-850A	11.0	811.46	1208.03	0.378	75.04
CD-500P-850A	10.2	0.26	0.38	0.391	59.43
PM-500P-850A	9.9	12.30	18.78	0.689	43.76
CM-500P-850A	11.7	5.65	8.73	0.743	22.42

3.3. Fourier Transform Infrared Spectroscopy (FTIR)

The FTIR spectra of biochar and activated biochar from coconut husks and various types of livestock manure are shown in Figure 4, and the FTIR spectral band assignments are shown in Table S1. The four unactivated biochars have obvious absorption peaks near

1450–1317 cm^{-1} , which are assigned to C–H bending vibrations [32]. Strong absorption peaks at 1000–1200 cm^{-1} may be ester-based stretching vibrations, and strong absorption peaks at 750–870 cm^{-1} belong to stretching vibrations of aromatic ring C–H or C–N, R–O–C, or R–O–CH₃ groups. After activation, the absorption peaks from functional groups on the CH biochar surface weaken, and it was not reprecipitated until the activation temperature increased to 850 °C, indicating enhanced aromaticity [33]. The infrared spectrum curves of CM and PM biochars change little after activation. When CD biochar is activated at 750 °C, obvious absorption peaks appear at 3443 cm^{-1} , 2933 cm^{-1} , and 1635 cm^{-1} . These are assigned to hydroxyl, C–H_n, and C=O stretching vibrations, respectively [34].

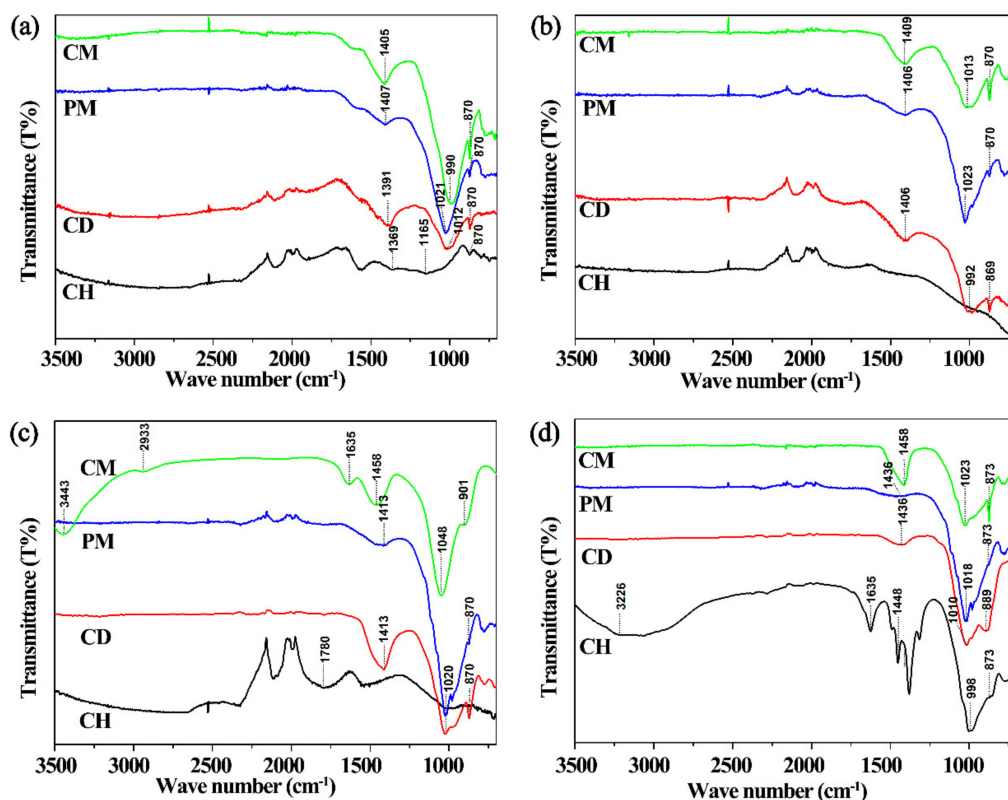


Figure 4. The FT-IR spectrum of (a) unactivated biochar samples; (b) biochar samples after activation at 650 °C; (c) biochar samples after activation at 750 °C; (d) biochar samples after activation at 850 °C.

3.4. Scanning Electron Microscopy

As shown in Figure 5, SEM is used to study microstructural and morphological changes to biomass precursors and biochar materials during pyrolysis and activation. Except for CM-500P, the biochars have looser structures after pyrolysis than before. The number of pores on the PM-500P and CH-500P surface increase, the size of pores becomes larger, and the shape of pores becomes round or oval. Although CH-500P and PM-500C have many pores on their surfaces, their pore diameter is about 2–15 μm . These pores cannot replace mesopores and micropores, and cannot adsorb H₂S effectively. The pores in CD-500P transition from long, narrow holes to round holes, and decrease in number during pyrolysis. CM-500P has few pores and maintains a compact structure during pyrolysis. SEM images of unactivated biochars are compared to those of biochars that have been activated for 90 min at 650 °C. The number of pores on the surfaces of CH-500P-650A and CD-500P-650A is reduced. The structures of PM-500P-650A and CM-500P-650A become more compact, and there are almost no pores on their surfaces. When the activation temperature is 750 °C, the structure of CH-500P-750A becomes looser and the pore size becomes larger, but the macropores that are present cannot adsorb H₂S directly. The surface

structures of CD-500P-750A, PM-500P-750A, and CM-500P-750A are more compact than those of their precursors, with few pores and no obvious distribution patterns. When the activation temperature is 850 °C, the surfaces of CH-500P-850A and CD-500P-850A are distributed with granular protrusions, and the number of surface pores is reduced further. PM-500P-850A and CM-500P-850A have almost no pores on their surfaces. This affects their H₂S removal performance characteristics substantially [35]. Therefore, simply increasing the activation temperature cannot increase the number of pores on the biochar surface, nor can it enhance the H₂S removal performance.

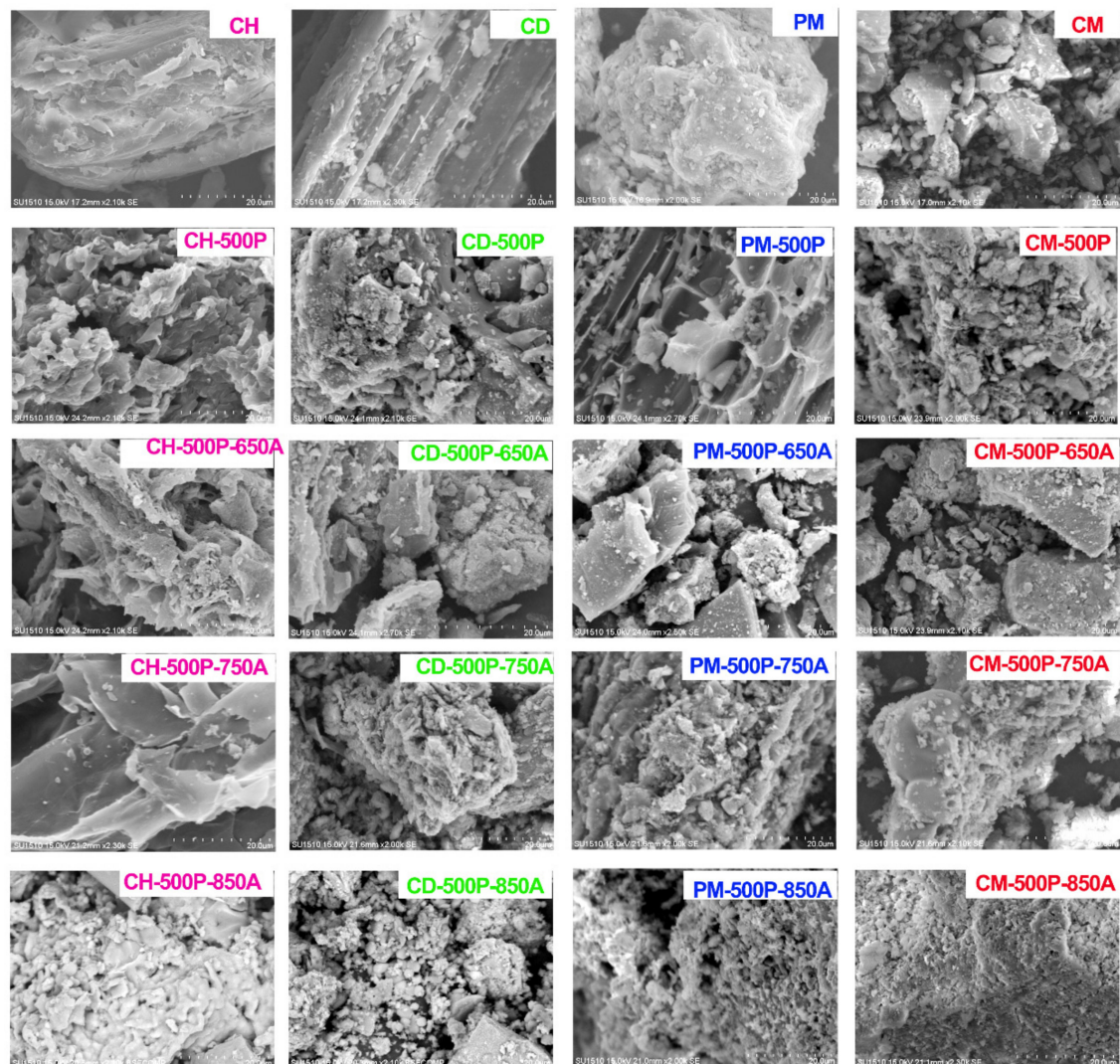


Figure 5. Scanning electron microscope images of coconut husks and various types of livestock manure before and after carbonation or activation.

3.5. Adsorption–Desorption Isotherms and Pore Size Distributions

In order to investigate the factors that influence biochar H₂S removal performance, we further characterize the pore size distributions and adsorption–desorption isotherms for these materials (Figures S1, S2 and S3). When the activation temperature is 650 °C, the CH-500P-650A and CD-500P-650A adsorption isotherms rise rapidly at low relative pressures ($P/P_0 < 0.1$). Above $P/P_0 > 0.1$, the curve rises slowly, indicating that the adsorption process is close to saturation. The N₂ adsorption isotherm fits a typical type I according to the IUPAC classification [36]. Thus, CH-500P-650A and CD-500P-650A contain large numbers of microporous structures. The PM-500P-650A and CM-500P-

650A adsorption isotherms exhibit inflection points at low pressure. This demonstrates that monolayer adsorption is saturated. A second adsorption layer begins to form as the pressure increases. This type II adsorption isotherm implies that pig manure biochar and chicken manure biochar are macroporous substances with few pores. When the activation temperature increases, CH-500P-750A and CH-500P-850A always exhibit type I adsorption isotherms, while CD-500P-750A, CD-500P-850A, CM-500P-750A, and CM-500P-850A always exhibit type II adsorption isotherms. PM-500P-750A exhibits a type I adsorption isotherm, which indicates that there are a certain number of micropores and mesopores in pig manure biochar. PM-500P-850A exhibits a type II isotherm, which indicates single multilayer adsorption on a macroporous solid [37].

3.6. H₂S Removal Performance of Biochar and Activated Product

Figure S4a shows the unactivated biochar H₂S breakthrough curve. Before activation, the penetration times for CH-500P and CD-500P are significantly longer than those for CW-500P and PW-500P. CH-500P exhibits the longest penetration time. With CD-500P and CH-500P, H₂S begins to be detected in the exhaust gas after 50 min and 70 min, respectively. Then, the H₂S concentration rises slowly, reaching the breakthrough concentration after about 70 min and 90 min, respectively. After activation at certain temperatures, the H₂S removal performances of CH-500P, CD-500P, and PM-500P improve (Figure 6a,c,e). The performance of CM decreases after activation, and further decreases monotonically as the activation temperature increases. After CD-500P is activated at 650 °C, the H₂S penetration time increases significantly; H₂S is detected at 75 min, and breakthrough occurs at 85 min. At this activation temperature, chicken manure biochar has the shortest H₂S adsorption penetration time. H₂S is detected in the exhaust gas at 20 min. The H₂S concentration rises rapidly and penetrates after 25 min. In the CH and PM H₂S adsorption tests, H₂S is detected in the exhaust gas after 70 min and 30 min, respectively. The H₂S concentration then increases slowly, reaching the breakthrough concentration after 80 min and 40 min, respectively. When the activation temperature rises to 750 °C, the CH-500P-750A breakthrough time increases significantly, becoming longer than CH biochar activated at other temperatures. H₂S is detected in the exhaust gas 100 min after the start of the test, and the penetration concentration is reached after 110 min. The breakthrough times for CD-500P-750A and CW-500P-750A are shortened significantly. H₂S is detected in the exhaust gas after 15 min and 5 min, respectively, and the breakthrough concentration is reached after 25 min and 10 min, respectively. The breakthrough time for PM-500P changes little. H₂S is detected after 35 min, and its breakthrough concentration is reached after 40 min. When the activation temperature is further increased to 850 °C, the CH-500P-850A breakthrough time is shortened, but the material still has the longest penetration time of the four samples. H₂S is detected in the exhaust gas 70 min after the start of the test, and the breakthrough concentration is reached after 75 min. The CD, PM, and CM breakthrough times are all shortened and the breakthrough concentration is reached within 5 to 15 min. The breakthrough time is shortest for CD.

The calculated H₂S removal capacities of various biochar samples are shown in Table 4, and the H₂S removal capacities histograms are shown in Figure S4b and Figure 6b,d,f. The H₂S removal capacities of various biochar materials do not increase with the activation temperature, and the manner in which the capacities vary is inconsistent. The biochar-derived activated samples with the best H₂S removal capacities and the corresponding values are: CH-500P-750A, 38.73 mg H₂S/g; CD-500P-650A, 38.23 mg H₂S/g; PM-500P-750A, 16.49 mg H₂S/g; and CM-500P 10.96 mg H₂S/g. The H₂S removal capacity of CD-500P-650A is equivalent to that of CH-500P-750A, which is 2.32 and 3.49 times that of PM-500P-750A and CM-500P, respectively, even though the activation temperature is 100 °C lower.

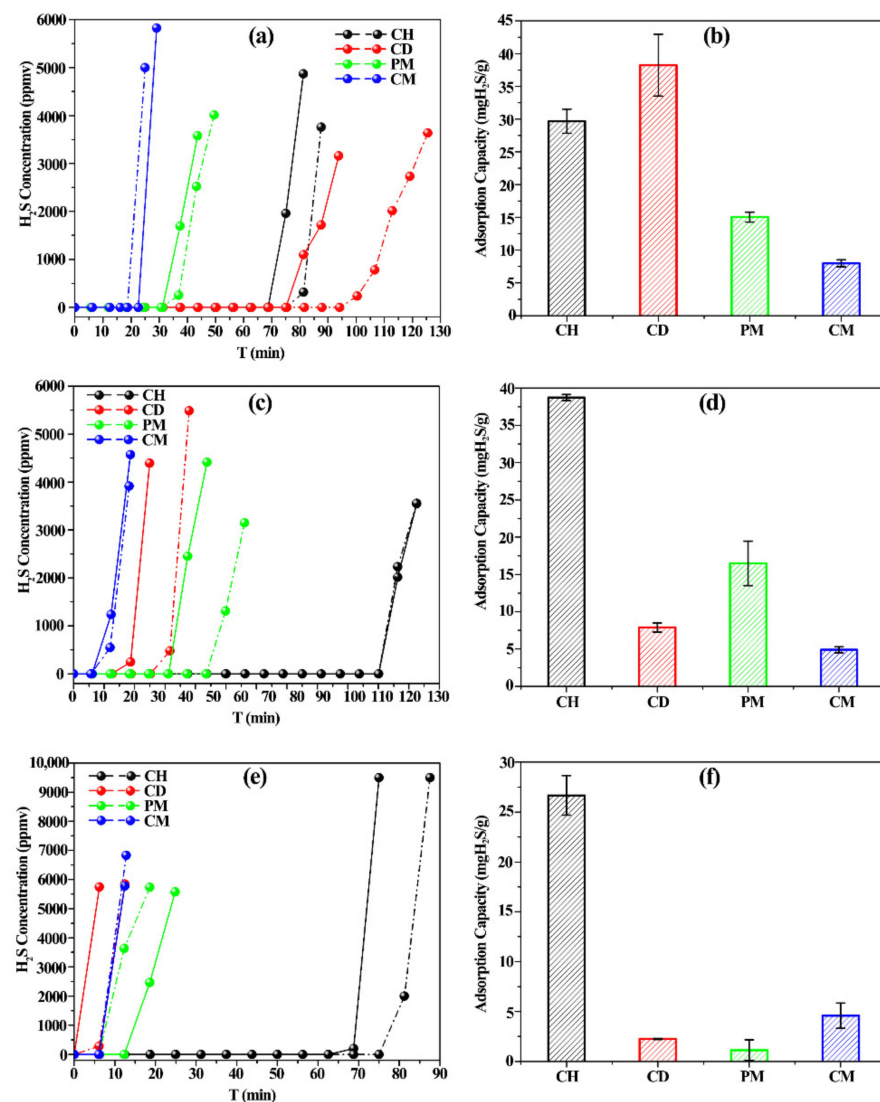


Figure 6. The H₂S breakthrough curve of activated biochar samples at various temperatures: (a) 650 °C; (c) 750 °C; (e) 850 °C; the H₂S removal capacities histogram of activated biochar samples at various temperatures: (b) 650 °C; (d) 750 °C; (f) 850 °C.

Table 4. H₂S removal capacities of biochar samples before and after activation.

Activation Temperature (°C)	CH (mg H ₂ S/g)	CD (mg H ₂ S/g)	PM (mg H ₂ S/g)	CM (mg H ₂ S/g)
/	30.44	29.81	13.82	10.96
650	29.68	38.23	15.03	7.98
750	38.73	7.87	16.49	4.90
850	26.67	1.13	4.57	2.25

In order to investigate the factors that affect biochar H₂S removal performance further, linear relationships between removal performance and the BET and Langmuir micropore surface areas were studied. Goodness-of-fit tests demonstrate that there is a power function relationship between the BET surface area, Langmuir micropore surface area, and biochar desulfurization performance. As Figure 7 shows, the trend lines fitted using processing software show that the R² values are 0.9693 and 0.9690 for the BET and Langmuir micropore surface areas, respectively. This demonstrates that the H₂S removal performance of biochar is not entirely dependent on the BET or micropore surface areas. We can combine these

results with analysis of the microscopic morphology and pore size distribution. The H₂S removal performance characteristics of biochars with microporous structures (CH-500P-650, 750, and 850A; CD-500P-650A; and PM-500P-750A) are better than those of biochars with large, mesoporous structures (CD-500P-750 and 850A; CM-500P-650, 750, and 850A; and PM-500P-650 and 850A). Thus, we conclude: (1) the micropores are responsible for most H₂S adsorption, while the macropores are responsible for transport of H₂S to the micropores; (2) simply increasing the activation temperature does not increase the number of pores on the biochar surface, nor does it enhance the biochar H₂S removal performance; (3) the H₂S removal performance of biochar is closely related to its microstructure and physicochemical properties.

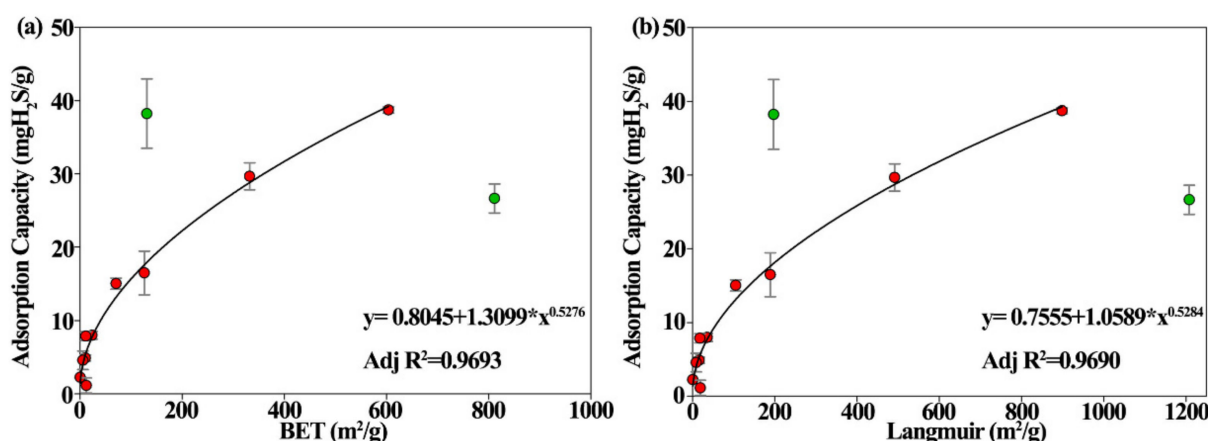


Figure 7. (a) The linear relationship curve between BET and biochar H₂S adsorption capacity; (b) the linear relationship curve between Langmuir micropore surface area and biochar H₂S adsorption capacity.

4. Conclusions

In this study, livestock manure and coconut husks were used as raw materials for biochar preparation via high-temperature pyrolysis, and the H₂S removal performance characteristics of the resulting biochar materials were evaluated. The effects of various activation temperatures on the microstructures and physicochemical properties of biochar materials were further investigated, and the H₂S removal performance of activated biochar was characterized. High-temperature pyrolysis under N₂ was used to convert CD, CM, and PM into biochar. Without activation, the desulfurization performances of the CD, CM, and PM biochars were 29.81 mg H₂S/g, 13.82 mg H₂S/g, and 10.96 mg H₂S/g, respectively. Of the materials tested, CD biochar had the highest H₂S removal performance, which was similar to that of CH biochar (30.44 mg H₂S/g). Biochar was physically activated using CO₂, and the effects of various activation temperatures and activation times on the biochar microstructure and H₂S removal properties were investigated. The study found that, after activation at 650 °C for 90 min, CD biochar had the highest H₂S removal performance (38.23 mg H₂S/g). This was an increase of 28.25% compared to the nonactivated materials. When the activation temperature was 750 °C, the H₂S removal performance of CH biochar was the highest at 38.73 mg H₂S/g. The H₂S removal performance was not only a function of the BET surface area, but was closely related to the pore size distribution. Most of the pores on the surface of CD biochar were micropores and, thus, conducive to H₂S adsorption. However, most of the pig and chicken manure biochar material surfaces had macroporous structures, which were not conducive to H₂S adsorption. This study suggests that CD biochar has broad prospects for application to H₂S removal from landfill gas.

Supplementary Materials: The following are available online at <https://www.mdpi.com/article/10.3390/su13116262/s1>, Figure S1: Adsorption–desorption isotherm and pore size distribution graph of biochar samples after activation at 650 °C. (a), (b) CH; (c), (d) CD; (e), (f) PM; (g), (h) CM. Figure S2:

Adsorption–desorption isotherm and pore size distribution graph of biochar samples after activation at 750 °C. (a), (b) CH; (c), (d) CD; (e), (f) PM; (g), (h) CM. Figure S3: Adsorption–desorption isotherm and pore size distribution graph of biochar samples after activation at 850 °C. (a), (b) CH; (c), (d) CD; (e), (f) PM; (g), (h) CM. Figure S4: (a) The H₂S breakthrough curve of unactivated biochar samples; (b) The H₂S removal capacities histogram of unactivated biochar samples. Table S1: FTIR spectral band assignments for biochar and activated biochar from different types of livestock manure and coconut husks.

Author Contributions: Conceptualization, L.S.; data curation, M.Z.; formal analysis, M.C.; funding acquisition, L.Z. and H.L.; investigation, G.Z. and M.Z.; software, R.J.; writing—original draft, S.W.; writing—review and editing, S.W. All authors have read and agreed to the published version of the manuscript.

Funding: This research was funded by Innovative team project of Nanjing Institute of Environmental Sciences, Ministry of Ecology and Environment (GYZX210101) and the International Science & Technology Cooperation Program (No. 2015DFA91390).

Institutional Review Board Statement: Not applicable.

Informed Consent Statement: Not applicable.

Data Availability Statement: The data used to support the findings of this study are available from the corresponding author upon request.

Acknowledgments: The authors wish to thank the Innovative team project of Nanjing Institute of Environmental Sciences, Ministry of Ecology and Environment (GYZX210101) and the International Science & Technology Cooperation Program (No. 2015DFA91390). The funding sources had no role in the study design, data collection and analysis, decision to publish, or preparation of the manuscript.

Conflicts of Interest: The authors declare no conflict of interest.

References

- Jia, W.; Qin, W.; Zhang, Q.; Wang, X.; Ma, Y.; Chen, Q. Evaluation of crop residues and manure production and their geographical distribution in China. *J. Clean. Prod.* **2018**, *188*, 954–965. [[CrossRef](#)]
- Lee, H.-J.; Ryu, H.-D.; Lim, D.Y.; Chung, E.G.; Kim, K.; Lee, J.K. Characteristics of veterinary antibiotics in intensive livestock farming watersheds with different liquid manure application programs using UHPLC-q-orbitrap HRMS combined with on-line SPE. *Sci. Total Environ.* **2020**, *749*, 142375. [[CrossRef](#)]
- Kamilaris, A.; Engelbrecht, A.; Pitsillides, A.; Prenafeta-Boldú, F.X. Transfer of manure as fertilizer from livestock farms to crop fields: The case of Catalonia. *Comput. Electron. Agric.* **2020**, *175*, 105550. [[CrossRef](#)]
- Jiang, Y.; Liang, X.; Yuan, L.; Nan, Z.; Deng, X.; Wu, Y.; Ma, F.; Diao, J. Effect of livestock manure on chlortetracycline sorption behaviour and mechanism in agricultural soil in Northwest China. *Chem. Eng. J.* **2021**, *415*, 129020. [[CrossRef](#)]
- Wu, R.-T.; Cai, Y.-F.; Chen, Y.-X.; Yang, Y.-W.; Xing, S.-C.; Liao, X.-D. Occurrence of microplastic in livestock and poultry manure in South China. *Environ. Pollut.* **2021**, *277*, 116790. [[CrossRef](#)]
- Adánez-Rubio, I.; Fonts, I.; de Blas, P.; Viteri, F.; Gea, G.; Alzueta, M.U. Exploratory study of polycyclic aromatic hydrocarbons occurrence and distribution in manure pyrolysis products. *J. Anal. Appl. Pyrolysis* **2021**, *155*, 105078. [[CrossRef](#)]
- Atienza-Martínez, M.; Ábrego, J.; Gea, G.; Marías, F. Pyrolysis of dairy cattle manure: Evolution of char characteristics. *J. Anal. Appl. Pyrolysis* **2020**, *145*, 104724. [[CrossRef](#)]
- Khoshnevisan, B.; Duan, N.; Tsapekos, P.; Awasthi, M.K.; Liu, Z.; Mohammadi, A.; Angelidaki, I.; Tsang, D.C.W.; Zhang, Z.; Pan, J.; et al. A critical review on livestock manure biorefinery technologies: Sustainability, challenges, and future perspectives. *Renew. Sustain. Energy Rev.* **2021**, *135*, 110033. [[CrossRef](#)]
- Zubair, M.; Wang, S.; Zhang, P.; Ye, J.; Liang, J.; Nabi, M.; Zhou, Z.; Tao, X.; Chen, N.; Sun, K.; et al. Biological nutrient removal and recovery from solid and liquid livestock manure: Recent advance and perspective. *Bioresour. Technol.* **2020**, *301*, 122823. [[CrossRef](#)] [[PubMed](#)]
- Liu, Z.; Wang, Z.; Tang, S.; Liu, Z. Fabrication, characterization and sorption properties of activated biochar from livestock manure via three different approaches. *Resour. Conserv. Recycl.* **2021**, *168*, 105254. [[CrossRef](#)]
- Ershadi, S.Z.; Dias, G.; Heidari, M.D.; Pelletier, N. Improving nitrogen use efficiency in crop-livestock systems: A review of mitigation technologies and management strategies, and their potential applicability for egg supply chains. *J. Clean. Prod.* **2020**, *265*, 121671. [[CrossRef](#)]
- Akdeniz, N. A systematic review of biochar use in animal waste composting. *Waste Manag.* **2019**, *88*, 291–300. [[CrossRef](#)]
- Song, J.; Wang, Y.; Zhang, S.; Song, Y.; Xue, S.; Liu, L.; Lvy, X.; Wang, X.; Yang, G. Coupling biochar with anaerobic digestion in a circular economy perspective: A promising way to promote sustainable energy, environment and agriculture development in China. *Renew. Sustain. Energy Rev.* **2021**, *144*, 110973. [[CrossRef](#)]

14. Romero, C.M.; Li, C.; Owens, J.; Ribeiro, G.O.; McAllister, T.A.; Okine, E.; Hao, X. Nutrient cycling and greenhouse gas emissions from soil amended with biochar-manure mixtures. *Pedosphere* **2021**, *31*, 289–302. [[CrossRef](#)]
15. Song, H.-J.; Kim, S.; Cho, Y. Removal of heavy metals using sorbents derived from bark. *J. Porous Mater.* **2020**, *27*, 319–328. [[CrossRef](#)]
16. Sulok, K.M.T.; Ahmed, O.H.; Khew, C.Y.; Zehnder, J.A.M.; Jalloh, M.B.; Musah, A.A.; Abdu, A. Chemical and Biological Characteristics of Organic Amendments Produced from Selected Agro-Wastes with Potential for Sustaining Soil Health: A Laboratory Assessment. *Sustainability* **2021**, *13*, 4919. [[CrossRef](#)]
17. Meier, S.; Curaqueo, G.; Khan, N.; Bolan, N.; Cea, M.; Eugenia, G.M.; Cornejo, P.; Ok, Y.S.; Borie, F. Chicken-manure-derived biochar reduced bioavailability of copper in a contaminated soil. *J. Soil. Sediment.* **2017**, *17*, 741–750. [[CrossRef](#)]
18. Yu, G.; Wu, X.; Wei, L.; Zhou, Z.; Liu, W.; Zhang, F.; Qu, Y.; Ren, Z. Desulfurization of diesel fuel by one-pot method with morpholinium-based Brønsted acidic ionic liquid. *Fuel* **2021**, *296*, 120551. [[CrossRef](#)]
19. Neubauer, R.; Weinlaender, C.; Kienzl, N.; Bitschnau, B.; Schroettner, H.; Hochenauer, C. Adsorptive on-board desulfurization over multiple cycles for fuel-cell-based auxiliary power units operated by different types of fuels. *J. Power Sources* **2018**, *385*, 45–54. [[CrossRef](#)]
20. El-hoshoudy, A.N.; Soliman, F.S.; Abd El-Aty, D.M. Extractive desulfurization using choline chloride-based DES/molybdate nanofluids; Experimental and theoretical investigation. *J. Mol. Liq.* **2020**, *318*, 114307. [[CrossRef](#)]
21. Saha, B.; Vedachalam, S.; Dalai, A.K. Review on recent advances in adsorptive desulfurization. *Fuel Process. Technol.* **2021**, *214*, 106685. [[CrossRef](#)]
22. Choudhury, A.; Lansing, S. Biochar addition with Fe impregnation to reduce H₂S production from anaerobic digestion. *Biore-sour. Technol.* **2020**, *306*, 123121. [[CrossRef](#)] [[PubMed](#)]
23. Hervy, M.; Pham Minh, D.; Gérente, C.; Weiss-Hortala, E.; Nzihou, A.; Villot, A.; Le Coq, L. H₂S removal from syngas using wastes pyrolysis chars. *Chem. Eng. J.* **2018**, *334*, 2179–2189. [[CrossRef](#)]
24. Yang, E.; Yao, C.; Liu, Y.; Zhang, C.; Jia, L.; Li, D.; Fu, Z.; Sun, D.; Robert Kirk, S.; Yin, D. Bamboo-derived porous biochar for efficient adsorption removal of dibenzothiophene from model fuel. *Fuel* **2018**, *211*, 121–129. [[CrossRef](#)]
25. Jung, S.; Kim, J.-H.; Lee, D.-J.; Lin, K.-Y.A.; Tsang, Y.F.; Yoon, M.-H.; Kwon, E.E. Virtuous utilization of biochar and carbon dioxide in the thermochemical process of dairy cattle manure. *Chem. Eng. J.* **2021**, *416*, 129110. [[CrossRef](#)]
26. Awasthi, S.K.; Duan, Y.; Liu, T.; Zhou, Y.; Qin, S.; Liu, H.; Varjani, S.; Awasthi, M.K.; Zhang, Z.; Pandey, A.; et al. Sequential presence of heavy metal resistant fungal communities influenced by biochar amendment in the poultry manure composting process. *J. Clean. Prod.* **2021**, *291*, 125947. [[CrossRef](#)]
27. Li, X.; Zhan, Y.; Su, L.; Chen, Y.; Chen, M.; Zhang, L.; Zhen, G.; Han, Z.; Chai, X. Sequestration of Sulphide from Biogas by thermal-treated iron nanoparticles synthesized using tea polyphenols. *Environ. Technol.* **2020**, *41*, 741–750. [[CrossRef](#)]
28. Su, L.; Liu, C.; Liang, K.; Chen, Y.; Zhang, L.; Li, X.; Han, Z.; Zhen, G.; Chai, X.; Sun, X. Performance evaluation of zero-valent iron nanoparticles (NZVI) for high-concentration H₂S removal from biogas at different temperatures. *RSC Adv.* **2018**, *8*, 13798–13805. [[CrossRef](#)]
29. Maljaee, H.; Madadi, R.; Paiva, H.; Tarelho, L.; Ferreira, V.M. Incorporation of biochar in cementitious materials: A roadmap of biochar selection. *Constr. Build. Mater.* **2021**, *283*, 122757. [[CrossRef](#)]
30. Zhang, Y.; Kawasaki, Y.; Oshita, K.; Takaoka, M.; Minami, D.; Inoue, G.; Tanaka, T. Economic assessment of biogas purification systems for removal of both H₂S and siloxane from biogas. *Renew. Energy* **2021**, *168*, 119–130. [[CrossRef](#)]
31. Wang, X.; Zhai, M.; Guo, H.; Panahi, A.; Dong, P.; Levendis, Y.A. High-temperature pyrolysis of biomass pellets: The effect of ash melting on the structure of the char residue. *Fuel* **2021**, *285*, 119084. [[CrossRef](#)]
32. Lu, Z.; Zhang, H.; Shahab, A.; Zhang, K.; Zeng, H.; Bacha, A.-U.-R.; Nabi, I.; Ullah, H. Comparative study on characterization and adsorption properties of phosphoric acid activated biochar and nitrogen-containing modified biochar employing Eucalyptus as a precursor. *J. Clean. Prod.* **2021**, *12*, 127046. [[CrossRef](#)]
33. Peter, A.; Chabot, B.; Loranger, E. Enhanced activation of ultrasonic pre-treated softwood biochar for efficient heavy metal removal from water. *J. Environ. Manag.* **2021**, *290*, 112569. [[CrossRef](#)]
34. Yao, Q.; Borjihan, Q.; Qu, H.; Guo, Y.; Zhao, Z.; Qiao, L.; Li, T.; Dong, A.; Liu, Y. Cow dung-derived biochars engineered as antibacterial agents for bacterial decontamination. *J. Environ. Sci.* **2021**, *105*, 33–43. [[CrossRef](#)]
35. Ma, Q.; Chen, W.; Jin, Z.; Chen, L.; Zhou, Q.; Jiang, X. One-step synthesis of microporous nitrogen-doped biochar for efficient removal of CO₂ and H₂S. *Fuel* **2021**, *289*, 119932. [[CrossRef](#)]
36. Maziarka, P.; Wurzer, C.; Arauzo, P.J.; Dieguez-Alonso, A.; Mašek, O.; Ronsse, F. Do you BET on routine? The reliability of N₂ physisorption for the quantitative assessment of biochar's surface area. *Chem. Eng. J.* **2021**, *418*, 129234. [[CrossRef](#)]
37. Wang, C.; Li, L.; Shi, J.; Jin, H. Biochar production by coconut shell gasification in supercritical water and evolution of its porous structure. *J. Anal. Appl. Pyrolysis* **2021**, *156*, 105151. [[CrossRef](#)]